

# We are IntechOpen, the world's leading publisher of Open Access books Built by scientists, for scientists

**4,800**

Open access books available

**122,000**

International authors and editors

**135M**

Downloads

Our authors are among the

**154**

Countries delivered to

**TOP 1%**

most cited scientists

**12.2%**

Contributors from top 500 universities



**WEB OF SCIENCE™**

Selection of our books indexed in the Book Citation Index  
in Web of Science™ Core Collection (BKCI)

Interested in publishing with us?  
Contact [book.department@intechopen.com](mailto:book.department@intechopen.com)

Numbers displayed above are based on latest data collected.

For more information visit [www.intechopen.com](http://www.intechopen.com)



# Novel Digital Magnetometer for Atmospheric and Space Studies (DIMAGORAS)

George Dekoulis

*Space Plasma Environment and Radio Science Group, Lancaster University  
United Kingdom*

## 1. Introduction

This chapter describes the design and scientific results from a new tri-axial magnetometer for atmospheric and space studies. The new instrumentation features multi-frequency (1 KHz - 1.5 MHz), multi-bandwidth (1 Hz - 10 KHz), multi magnetic field measurement range, low-power and re-configurable operation. This novel architecture is based on producing a programmable receiver independent of the fluxgate sensor used. Any ring-core, race-track or parallel type fluxgate sensor may be connected to the input and a working system is produced within hours. The current implementation is based on a novel shielded 3-dimensional sensor optimised for previously unseen low-power consumption compared to existing tri-axial macro-sensors. As a fully digital system the sensor's output is sampled after the amplification stage.

The full extent of the complex solar wind - magnetospheric - ionospheric system is measured by the magnetometer, due to the receiver's programmable dynamic range (DR) and the programmable cross-correlator integration time. The field-programmable gate array (FPGA) hardware implementation yields to a programmable filtering scheme that selects different centre frequencies and desired signal bandwidths. The output is directly in nT to avoid any unnecessary software post-processing calibration procedures and to ensure compatibility of results amongst users. The user selects either the magnetic field's vector components or the total intensity to be present at either the universal asynchronous receiver and transmitter (UART) or the fast 10/100 Mbps Ethernet communications ports.

The development of the magnetometer's sensor is based on the implementation of a novel design methodology for producing optimised fluxgate sensors for low-power consumption. The sensor is qualified for both ground-based and spaceborne observations. The results are of interest to the aerospace and defence industries, since fluxgate sensors exist in airborne and spaceborne systems for decades. Lowering power consumption is followed by simplification of the accompanying electronic circuits.

The system is constantly being enriched by research results from an ongoing collaboration with NASA's Jet Propulsion Laboratory (JPL) on a different project for future missions (Dekoulis & Murphy, 2008). The presented system is complementing existing and under development state-of-the-art systems, such as, scalar/vector magnetometers. The system acts as a pathfinder for future high-resolution planetary exploration missions.

## 2. Sensors and magnetometers

Fluxgate sensors and magnetometers are used to measure the Earth's magnetic field. Currently, the research conducted on sensors is based on miniaturisation by using new materials. Non-semiconductor sensors, such as fluxgates, induction sensors etc. are already using micro-technologies. Micro-coils and micro-relays are using modern micromachining processes (Seidemann et al., 2000). Amorphous materials such as wires and tapes are applied to sensors (Meydan, 1995).

Within the Space Physics context, magnetic fields of interest are the galactic magnetic field ( $B \approx 0.2$  nT), Earth's magnetic field ( $B \approx 60$  uT), white dwarf's ( $B \approx 1$  KT) and pulsar's ( $B \approx 100$  MT). At the poles the field has a 90-degree inclination and magnitude of 60 uT. At the equator the field has 0 degrees inclination and magnitude of 30 uT. There are anomalous cases where the field is 180 uT vertical (Kursk, Russia) and 360 uT vertical (Kiruna, Sweden). Other anomalies are created due to the magnetisation of the rocks and human ferromagnetic structures that could affect communications. During a day the magnetic field fluctuates between 10 - 100 nT, due to solar radiation and the induced ionisation of the ionosphere. The observed micro-pulsations have periods of 10 ms - 1 h and amplitudes up to  $10\gamma$ . Magnetic storms happen frequently within a month, last for couple of days and exhibit amplitudes of few hundreds of nT.

After extensive analysis of the available technologies, the choice was between the ring-core and race-track sensors. Race track sensors have lower demagnetisation factor, higher directional sensitivity, less sensitivity to orthogonal fields (interference). Race-track sensors exhibit large unbalanced spurious signals and problems from higher tape pressure in the corners. Ring-core sensors have an anuloid excitation coil and a solenoid-sensing coil. Although they have low sensitivity due to the demagnetisation, ring-core designs have many advantages and produce low-noise sensors. Rotating the core with respect to the sensing coil permits precision balancing of the core symmetry. Ring-core sensors exhibit uniform distribution of any mechanical stress. The increased noise associated with open-ended rods is absent. Tape ends are a insignificant source of noise. Sensitivity is proportional to the sensor diameter. For a given diameter, a trial-by-error procedure was followed to determine the optimum for the other dimensions.

In geophysical measurements the scalar resonance magnetometers are used. Overhauser magnetometers have replaced the classic proton magnetometers. Optical magnetometers are used for airborne applications. Similarly to this project, if 3-axial vector measurements are required, fluxgate magnetometers are used.

## 3. Magnetometers' design study

A fluxgate magnetometer with a ring-core sensor is to be designed. Comparison of existing sensor and magnetometer designs determined the optimum specifications of the novel digital magnetometer (Dekoulis & Honary, 2007).

A review on analogue fluxgates is in (Dekoulis, 2007). The major components of the second harmonic fluxgate magnetometer are presented in the block diagram of Fig. 1. A frequency generator generates the  $f$  and  $2f$  frequencies. The  $f$  frequency is a sine-wave or a square-wave between 400 Hz - 100 KHz and excites the sensor. For crystalline core materials a 5 KHz square-wave is used. The power amplifier is a totem-pole pair of hexfet transistors. The  $2f$  signal switches the phase-sensitive detector (PSD). The sensor output is amplitude modulated by the Earth's magnetic field and the PSD demodulates it to dc. The analogue

feedback has a large gain, so the sensor functions as a zero indicator. The current output of the voltage-to-current (V/I) converter is used to increase the DR of the instrument and is the current into the compensation coil. The feedback gain controls the sensor's nonlinearity and sensitivity. The sensor coil has roughly 2000 turns. Pre-amplification and bandpass filtering prior to PSD is required to filter the first harmonic and other spurious signals present at the sensor's output. The integrator is used to provide sufficient amplification (Pallas-Areny et al., 1991). The first digital fluxgate magnetometer (Primdahl et al., 1994) verifies that digital technology can be employed into magnetometry. The first real-time fluxgate magnetometer using FPGAs was made by Max-Planck Institute (Auster et al., 1995). A digital fluxgate magnetometer was added to the instrumentation of the Swedish satellite Astrid 2 (Pedersen et al., 1999).

Another solution is presented by (Kawahito et al., 1999). An analogue switching type synchronous detector was used connecting to an analogue integrator and a second order delta sigma modulator. A one-bit digital-to analogue converter was used to close the magnetic feedback loop. The 1-bit DAC guarantees linearity. The output of the DAC is connected to an analogue low-pass filter. The disadvantage with this system is the excessive noise of the device because the magnetic circuit was also implemented on the same device where the digital signal processing electronics were also implemented.

High-performance amorphous ferromagnetic ribbons were integrated on silicon wafers using CMOS manufacturing techniques and batch integration post-process of the ferromagnetic cores to create a 2-D fluxgate for electronic compass applications (Chiezi et al., 2000). The two cores are placed diagonally above the single square driving coil and the sensor is equivalent to a parallel type. However, the significant error of  $1.5^\circ$  ( $0.5 \mu\text{T}$ ) makes the system inaccurate even for electronic compass applications.

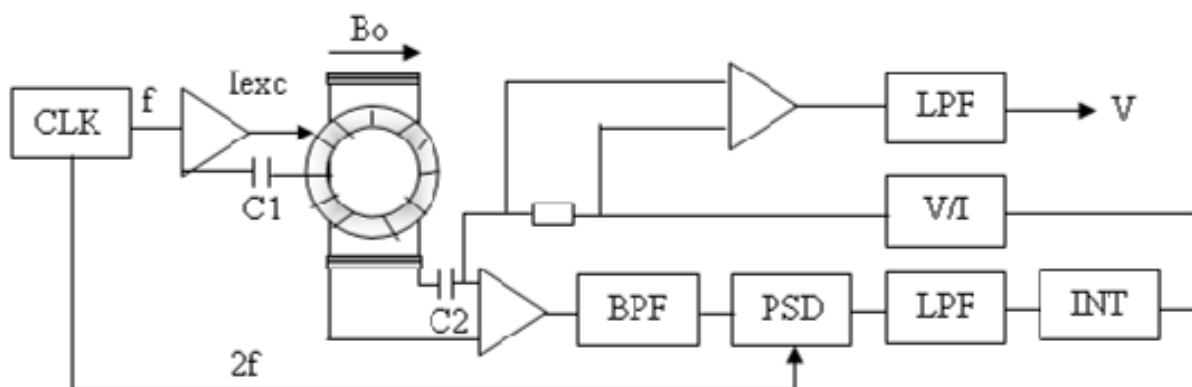


Fig. 1. Second Harmonic Fluxgate Magnetometer.

Space mission results are in the range of  $5 \text{ pT} - 2 \text{ mT}$ , with a typical accuracy of  $1^\circ$ . High accuracy is required for mapping of planetary magnetic fields. The integration time for the correlated data is from 1 s to hundreds of samples per second (Ness, 1970). Most magnetometers are of the vector type. Scalar magnetometers measure only the magnitude the ambient field, not the direction. Scalar magnetometers were not considered for this study due to their different architecture, specifications and measurement results. Tri-axial vector magnetometers are widely used on balloons, sounding rockets and spacecrafts. The calibration process is based on known magnetic fields both in amplitude and phase. The specifications include their output for zero-field, scale factor, temperature stability, time drift, weight, power consumption, operating temperature range and radiation hardness. The

Earth's magnetic field has been mapped using vector magnetometers with a resolution of 5 nT and 3 arc-seconds.

Ground based magnetometers, such as the INTERMAGNET, EISCAT, SAMNET and IMAGE networks, couple the operation of spaceborne systems. The Sub-Auroral Magnetometer Network (SAMNET) is operated by Lancaster University. It consists of 13 tri-axial analogue fluxgate magnetometer stations. They use the double-rod parallel type sensors, encapsulated into epoxy material for increased temperature stability, mechanical stress relief and maintenance of the sensors orthogonal relation. Typical measurements of SAMNET include the determination of Pi2 pulsations.

The magnetometer design is rapidly changing and two categories of evolving designs are identified. The first category covers design of a new sensor and the receiver architecture is adjusted to the sensor to obtain acceptable results. In many cases, due to the nature of the sensor the complexity of the receiver is amazing. It seems that there is only one chance to get the receiver working and a high possibility that the results are inferior even compared to a conventional analogue magnetometer.

The second category encompasses designs using existing sensors that improve the receiver's architecture. However, these solutions are accompanied with extra complexity on the digital side, (e.g. three DSP devices for a vector magnetometer) which means lots of hardware, design time, testing time, unknown propagation delays, synchronisation problems, complicated calibration procedures, decreased reliability factors, higher power consumption, which may lead to extra temperature and noise increase, and offset drifts. Three independent communication ports to the host data acquisition system are required. In both cases the systems are considered to be hardwired, since they perform a specific function. This is a term used in the past for analogue electronics specifically and based on the research results it applies to both the recent digital systems, since there is no flexibility in terms of signal processing. The systems are tied to one sensor, one operating frequency and one specific bandwidth. Most of them are tied to one integration time, although there are cases where a variable integration time scheme is operated. This is justified for the measurement of the Earth's magnetic field, but not when the magnetometer is, also, used for the combined study of the complex solar wind - magnetospheric - ionospheric system. To perform a parametric experiment corresponds to more than one human's effort, significant design time, and possibility of new errors, extra cost and the system is still hardwired. Another disadvantage of the existing analogue and digital systems is the finite DR. In recent digital systems with ADC resolution of 16 bits, the DR is tied to a specific value (maximum 96 dB for a top design), since there is no control on the hardwired analogue electronics. Thus, magnetospheric events and the variance of magnetic fields at the DR edges are lost.

The proposed system implements an architecture where both the analogue and digital counterparts are programmable and controlled by a single controller embedded into the chosen hardware target. The next section is dedicated to the selection of the appropriate hardware implementation technology.

#### **4. Novel digital magnetometer DIMAGORAS**

The system presented in Fig. 2 features the following:

- Single chip solution.
- Any ring-core or parallel type fluxgate sensor can be connected to the receiver input.



- Multi-frequency (1 KHz-1.5 MHz).
- 16-bit ADC resolution.
- 3 MSPS maximum sampling rate.
- Multi-bandwidth (1 Hz - 10 KHz).
- Output in nT.
- Selection of the 3 magnetic fields components in magnetic coordinates or the total intensity.
- UART and Ethernet interfaces for data logging.
- Target axis alignment orthogonality is <0.5%.
- Programmable field range of +/- 100 uT.
- Programmable sensitivity of 150uV/nT.
- 96 dB DR expandable to 176 dB.
- Programmable Integration Time. Default is 1 s.
- Re-configurability within ms.
- GPS referenced clock generation.
- GPS UT data timestamping.
- Lengthy data logging or DMA transfers.
- Automatic calculation of the Earth's magnetic field, based on the current GPS location.
- System operation -55 ° -+85 ° C.
- Power consumption <790mW.
- Weight <400 g including the three-axis sensor.
- Digital output at zero field < +/-0.02V.
- Temperature stability per sensor < 0.1 nT/deg.
- Long-term drift: < 10 pT/day.
- Noise < 7 pT/  $\sqrt{\text{Hz}}$  @ 1Hz.
- 20-year life span at maximum ratings.
- The FPGA failure rate is less than 1/1,000,000. FPGAs are used for space magnetometers, due to their efficient radiation hardness properties
- Flexible prototyping platform for other space centre ground based magnetometers.
- INTERMAGNET and SAMNET compatibility.
- Low cost lightweight standalone unit.

#### 4.1 System description

The tri-axial sensor is made of high permeability supermalloy material for increased sensitivity and low power consumption. The excitation coil has roughly 28 turns, while each pickup coil 24 turns. The user controlled sensitivity of the magnetometer is 163  $\mu\text{V}/\text{nT}$  to cover the +/- 100,000 nT range of the Earth's magnetic field. For a system located away from the poles the Earth's field variations are smaller, so a smaller range, e.g. +/- 65,000 nT, may be selected.

The excitation waveform is FPGA controlled and set to 5 KHz. A transistor network is used to drive the excitation coil to saturation with a square-wave of peak-to-peak current of only 60 mA.

The pre-amplifier (PA) and programmable gain controller are set by default to a gain of 20 dB. The AGC also provides the necessary filtering of the input to keep the noise to low levels. The master controller of the FPGA accurately controls the AGC. The 16-bit AD7621

ADC samples the three signals. The ADC accepts a differential voltage input of  $\pm 2.5$  V. 16 bits provide maximum 96 dB of dynamic range. The AGC functionality is employed when specific thresholds are exceeded to further increase the resolution to a maximum value of 176 dB.

The coil's sensitivity established that no more than 90 dB of gain are needed. The signal from any sensor between 1 KHz - 1.5 MHz may be sampled. Most of the existing sensors reviewed are tuned between 8 KHz - 100 KHz. The ADC samples at 0.9 MHz for a sensor tuned at 100 KHz. Exceeding oversampling increases severely the internal noise.

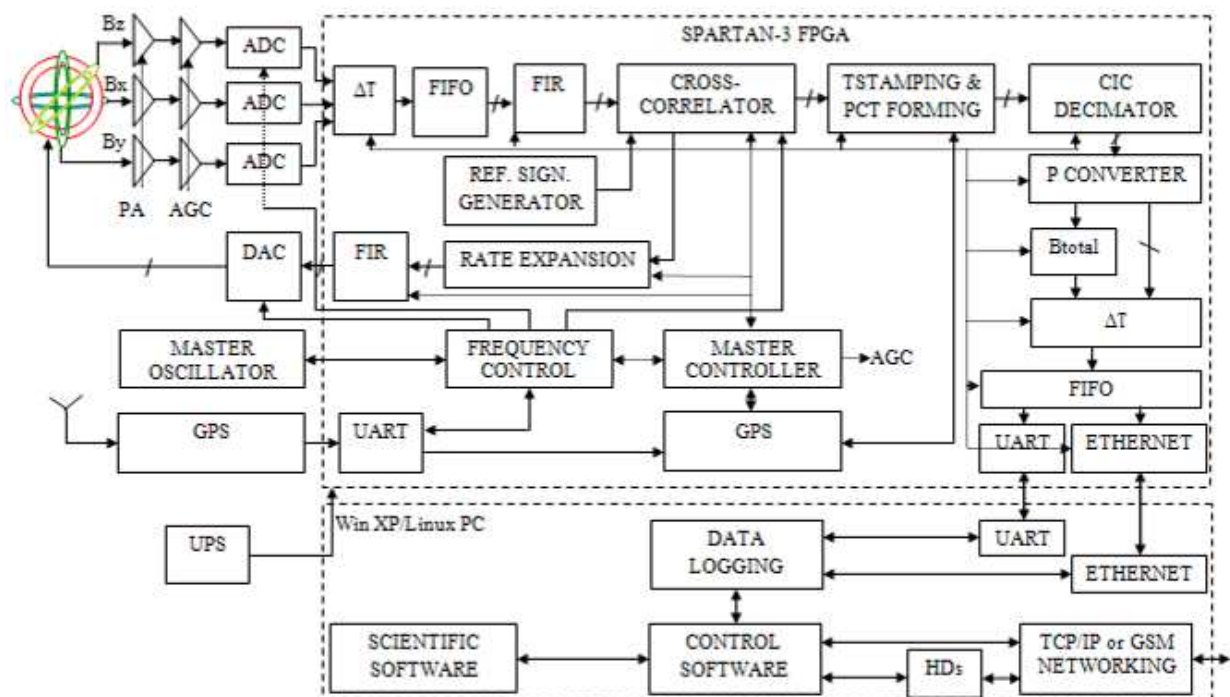


Fig. 2. DIMAGORAS Block Diagram.

The digital finite impulse response (FIR) filter extracts the second harmonic of the output, since all odd harmonics are eliminated due to the designed core structure. It partially controls the bandwidth by low-pass filtering the input signal at the third harmonic located at 15 KHz. The bandwidth is set from 1 Hz - 10 KHz. Most systems use a bandwidth of 10 Hz, which significantly increases the complexity of the FIR filter, compared to a 15 KHz filter.

More than one filtering stages are required to adjust the required bandwidth to a relative to the centre frequency low value. For a bandwidth of 10 KHz a single stage FIR filter is sufficient. For a bandwidth of 10 Hz, more than one stage is required. A set of four fully customisable CIC filters is used. A new bandwidth is set by reconfiguring the FPGA. The classical analogue phase sensitive detector has been implemented digitally to improve its performance.

A reference waveform is generated and multiplied with the output of the FIR filter. The reference waveform is similar to the pulse used to switch on and off the analogue PSD circuit. Values other than 0 and 1 are also used to recreate the sensor's characteristic.

The results of the cross-correlation are integrated for a default value of 1 s, similar to ARIES, IRIS and SAMNET. The outputs of the three integrators are timestamped, packeted and transmitted to the host. The GPS decoder extracts the accurate timing information from the GPS receiver and timestamps the data at the exact place where the measurements are taken. The interpolator and the FIR filter at the feedback loop are used to reduce the quantisation noise of the DAC.

The FIR filtering is effectively low-pass filtering the noise and limiting it to the system's bandwidth. The output of the decimator expresses a relative power measurement, which depends on the system's design characteristics. An internal calibration procedure assigns a fundamental relative power value to a magnetic field of known value, based on the sensitivity, gain, resolution and integration time. In this way, each axis output is translated into nT.

The user selects between the total intensity and individual constituents of the vector field. Decoding software extracts the field intensity and the timing information for each taken measurement. The PC runs the automation software for the production of the theoretical Earth's magnetic and the measured data is co-plotted for direct comparison.

#### 4.2 Sensor design

The novel sensor is in Fig. 3. Each xyz sensor is wound around two unused sides.

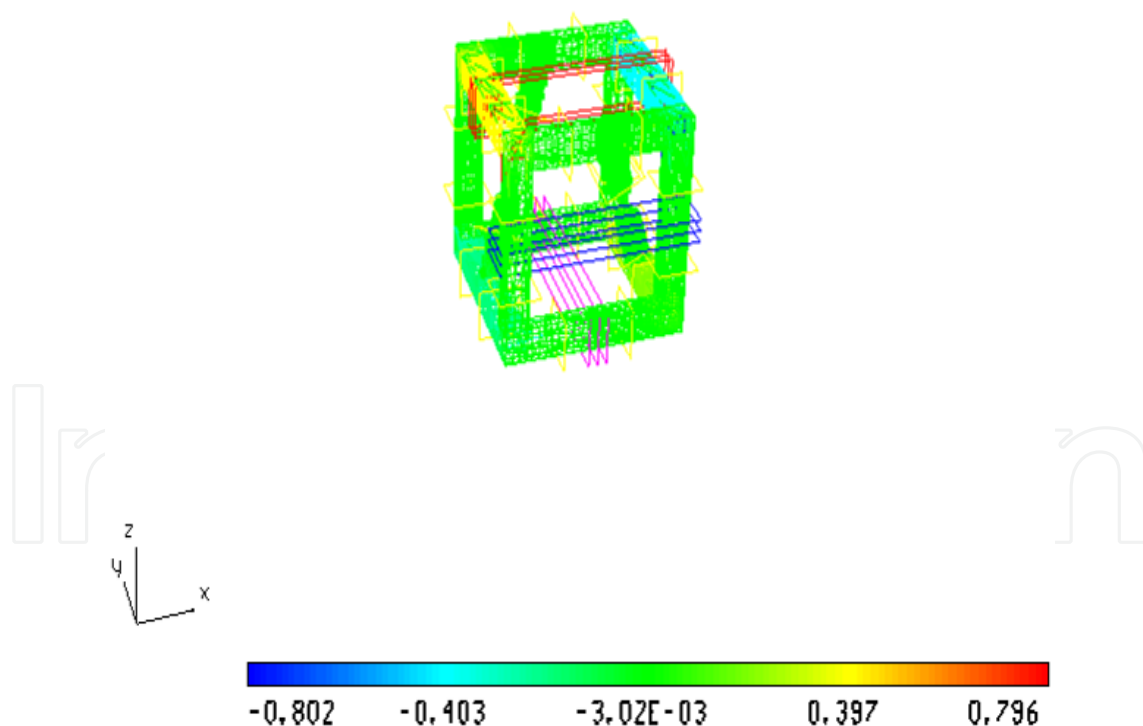


Fig. 3. The 3-D Dimagoras sensor and B Distribution ( $B_{sat} = 0.8$  T,  $I_{exc} = 60$  mA).

After following an extensive optimisation technique, the middle sections of the bottom right side are joined with the front topside and the bottom left side with the back topside of the structure using a suitable cone-link section (Dekoulis & Honary, 2008).



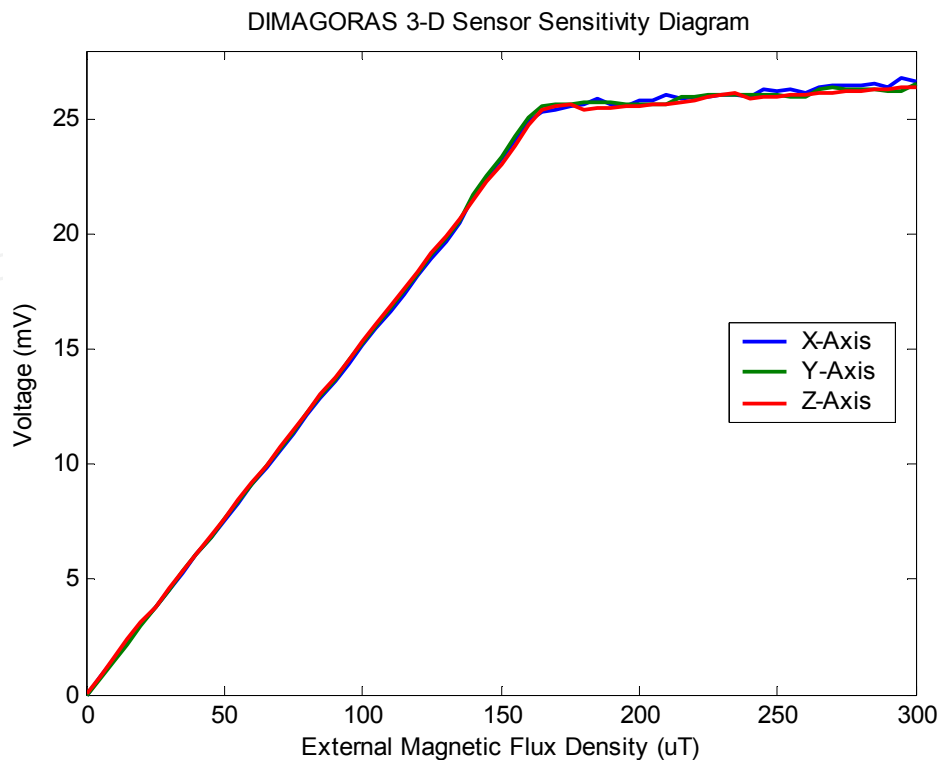


Fig. 4. 3-D Sensor's Sensitivity Diagram.

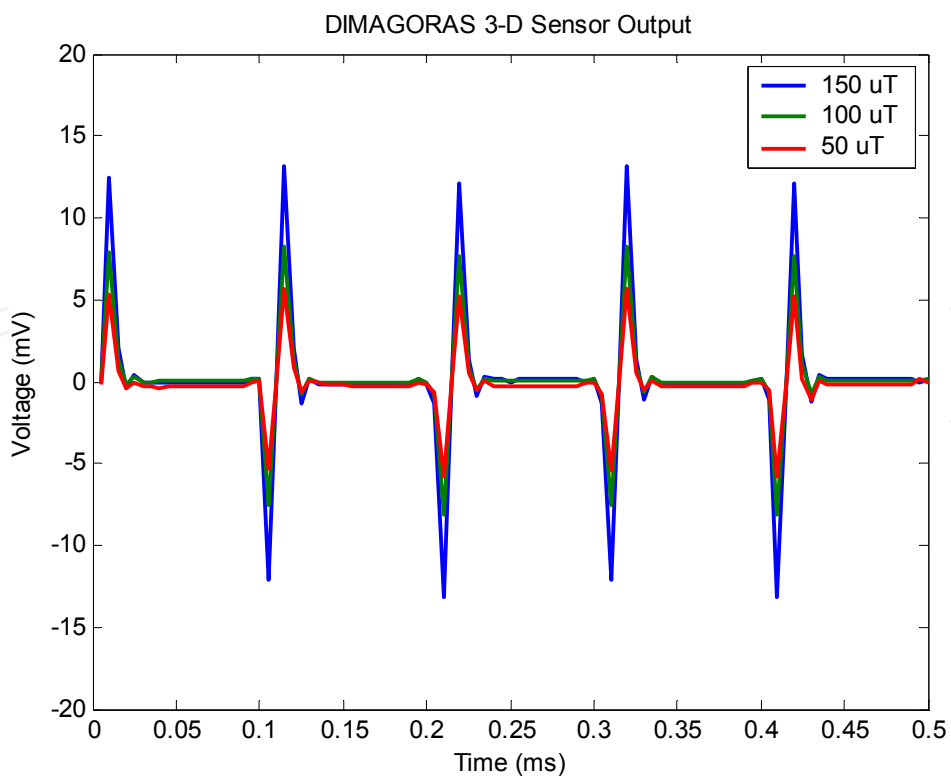


Fig. 5. 3-D Sensor's Output Response for  $B = 50, 100$  and  $150 \mu\text{T}$ .

The flux density distribution in the y-direction is shown in Fig. 3. Using 28 turns of excitation coil wrapped around the structure, the core is saturated at 0.8 T using a square-wave excitation current of +/- 60 mA at 5 KHz frequency. This is in complete harmony with the outcome of a similar optimisation procedure for the single-axis sensor.

The sensitivity diagram of the tri-axial sensor is plotted in Fig. 4. The measured sensitivity is 163  $\mu\text{V/nT}$ . The sensor's y-axis output response for an external field of 50, 100 and 150  $\mu\text{T}$  is in Fig. 5.  $V_{pp} = 25.2$  mV for  $B = 150$   $\mu\text{T}$ . The characteristic curve for the tri-axial sensor is in Fig. 6.

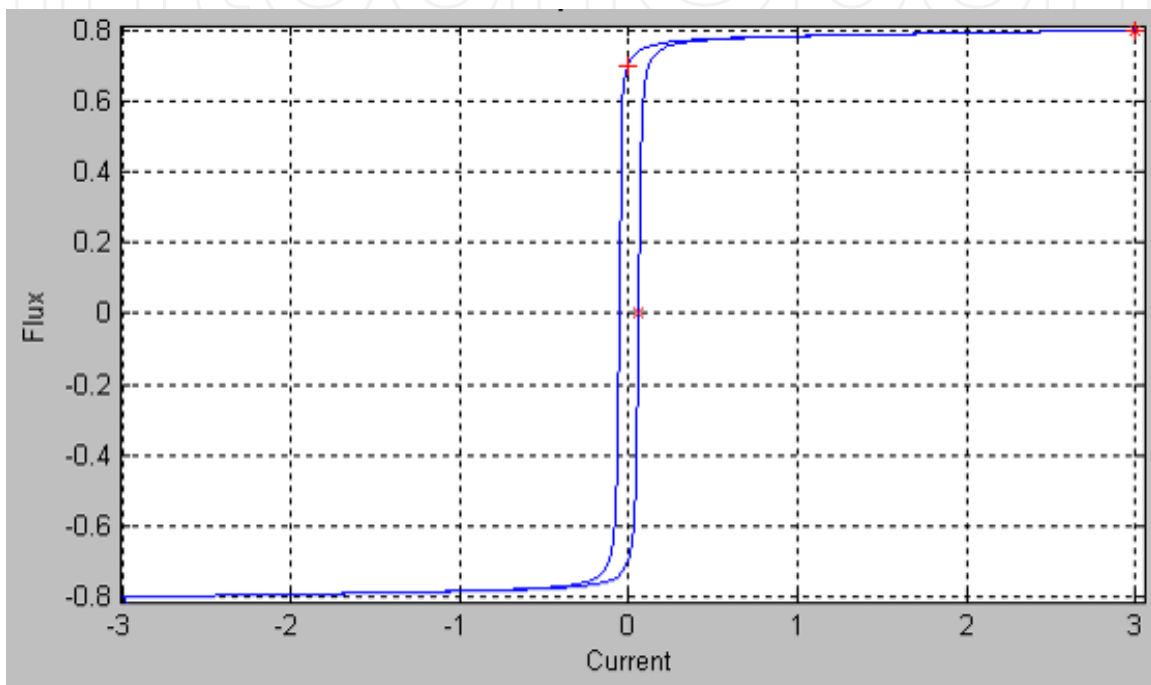


Fig. 6. Sensor's Magnetisation  $B(H)$  Curve (T(A/m)).

#### 4.3 Software design

The hardware prototype outputs the timestamped values in nT. This yielded to a reduction in software development time. The user selects the preferred interface, runs the logging software and the results are plotted in nT. This eliminates any calibration and scale adjustments. The power to nT curves are plotted in Fig. 7.

The circuit may be implemented as a decoder or the values may be stored directly into the Block RAM (BRAM) of the FPGA. Both solutions do not account for gain variations and adjustments are required before transmitting the results to the host. The final solution is based on a new real-time numerical approach. A fundamental curve has been produced by averaging the three calibration curves. The error of the derived curve with the original is less than 0.1 % and maximises for values within the saturation region. The error for the linear region is safely assumed to be 0. The curve is approximated by a square function in the linear region. The saturation region is approximated by a linear function. The circuit adapts the weights to pre-known intermediate or maximum values stored in the BRAM.

The total intensity  $B_T$  of the magnetic field (Macmillan et al., 1997) is calculated by eq. (1).

$$B_T = \sqrt{B_x^2 + B_y^2 + B_z^2} \quad (1)$$

where,  $B_x$ ,  $B_y$  and  $B_z$  are the external magnetic field intensities towards the north, east and zenith directions.

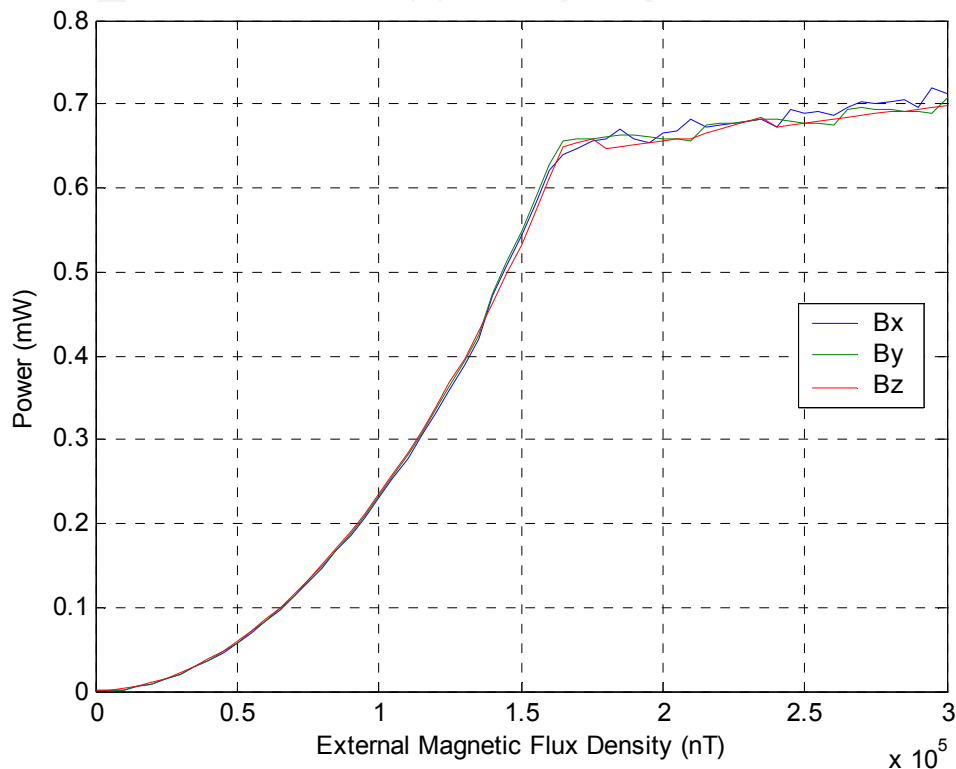


Fig. 7. Power to nT Curves for the 3-D Sensor.

The azimuth field intensity  $B_\phi$ , included in eq. (1), is given by eq. (2):

$$B_\phi = \sqrt{B_x^2 + B_y^2} \quad (2)$$

The inclination I and declination D are given by:

$$I = \arctan \frac{B_z}{B_\phi} \quad (3)$$

$$D = \arctan \frac{B_y}{B_x} \quad (4)$$

The final system implements eq. (1).

The system is SAMNET compatible (---, 2003). Data are recorded using one hour long files. Due to the improved capabilities of the digital magnetometer no further processing is required by the base, since the data are already in nT. The base may remotely choose

between the total intensity and the vector components, already expressed in magnetic coordinates.

The system was initially tested at Lancaster University  $54.01^\circ$  N latitude and  $2.77^\circ$  W longitude, as shown in Fig. 8.

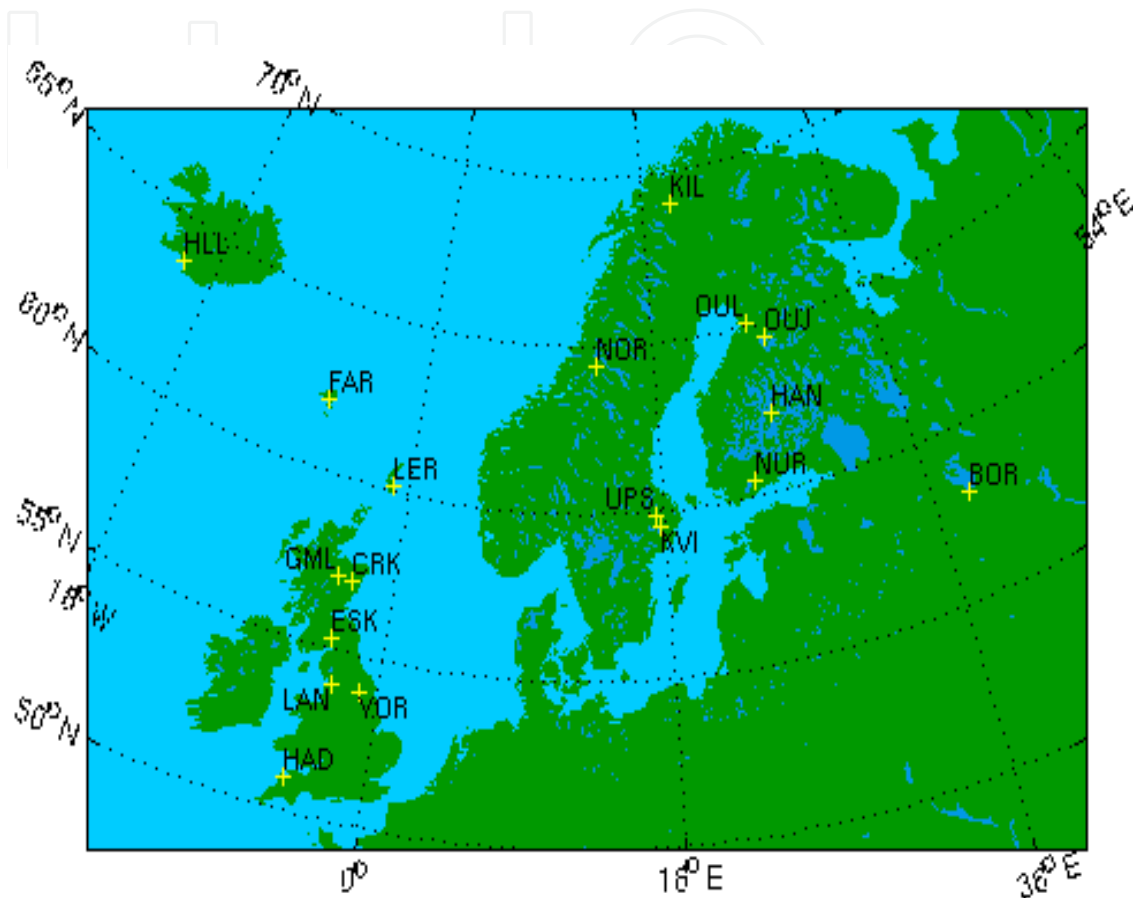


Fig. 8. SAMNET Locations.

Equations (5-11) apply for this geographical location on 28/5/2009.

$$D = -4.294^\circ \quad \text{changing by } 0.171^\circ/\text{year} \quad (5)$$

$$I = 70.635^\circ \quad \text{changing by } -0.005^\circ/\text{year} \quad (6)$$

$$B_x = 16520.85 \text{ nT} \quad \text{changing by } 18.63 \text{ nT}/\text{year} \quad (7)$$

$$B_y = 1240.43 \text{ nT} \quad \text{changing by } 48.3 \text{ nT}/\text{year} \quad (8)$$

$$B_z = 47137.77 \text{ nT} \quad \text{changing by } 30.25 \text{ nT}/\text{year} \quad (9)$$

$$B_\phi = 16567.35 \text{ nT} \quad \text{changing by } 15.04 \text{ nT}/\text{year} \quad (10)$$

$$B_T = 49964.46 \text{ nT} \quad \text{changing by } 33.52 \text{ nT}/\text{year} \quad (11)$$

The H component is plotted for all SAMNET stations in Fig. 9.

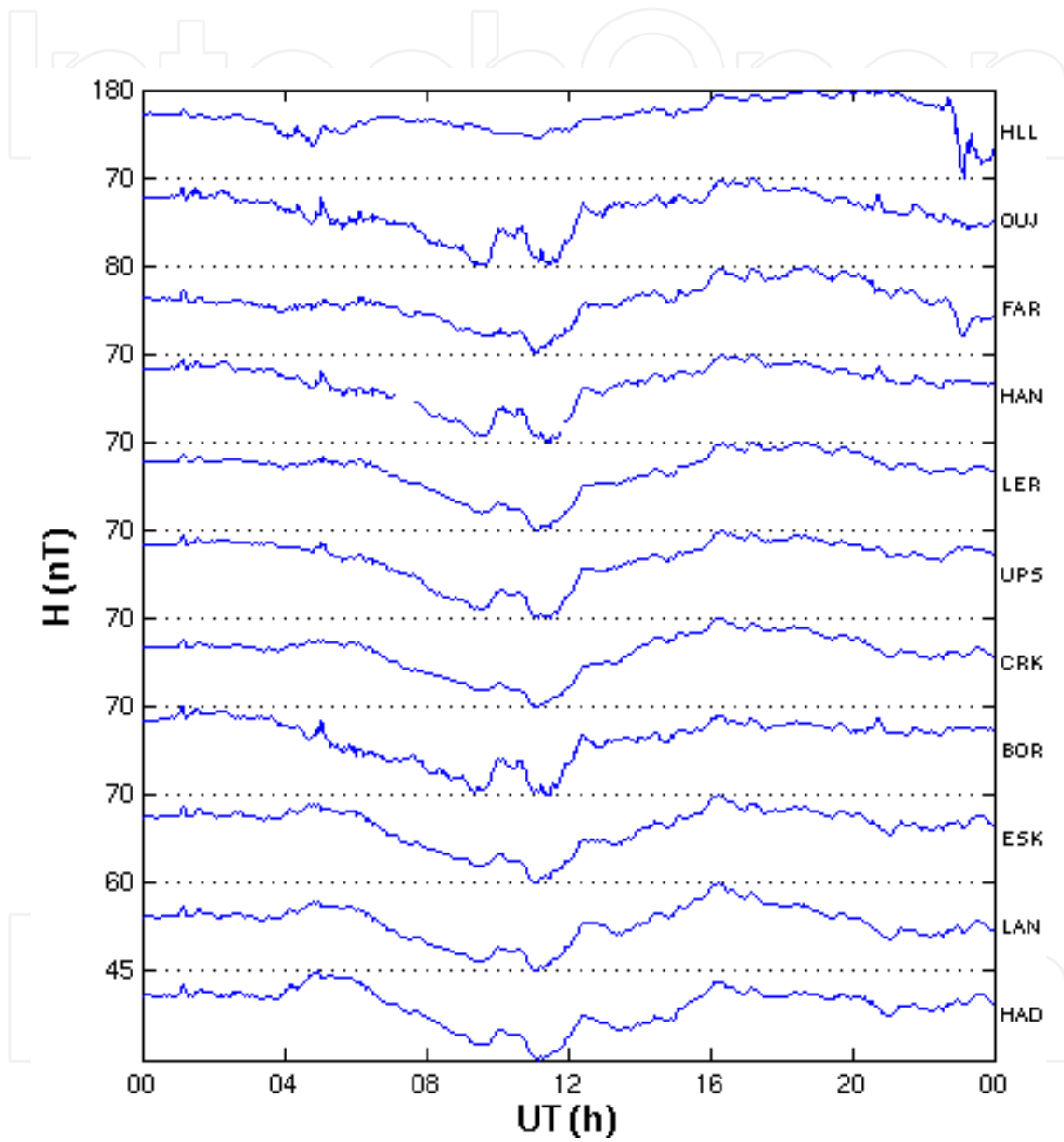


Fig. 9. H-Component SAMNET Magnetogram.



The D component is similarly plotted for all SAMNET stations for the same day in Fig. 10.

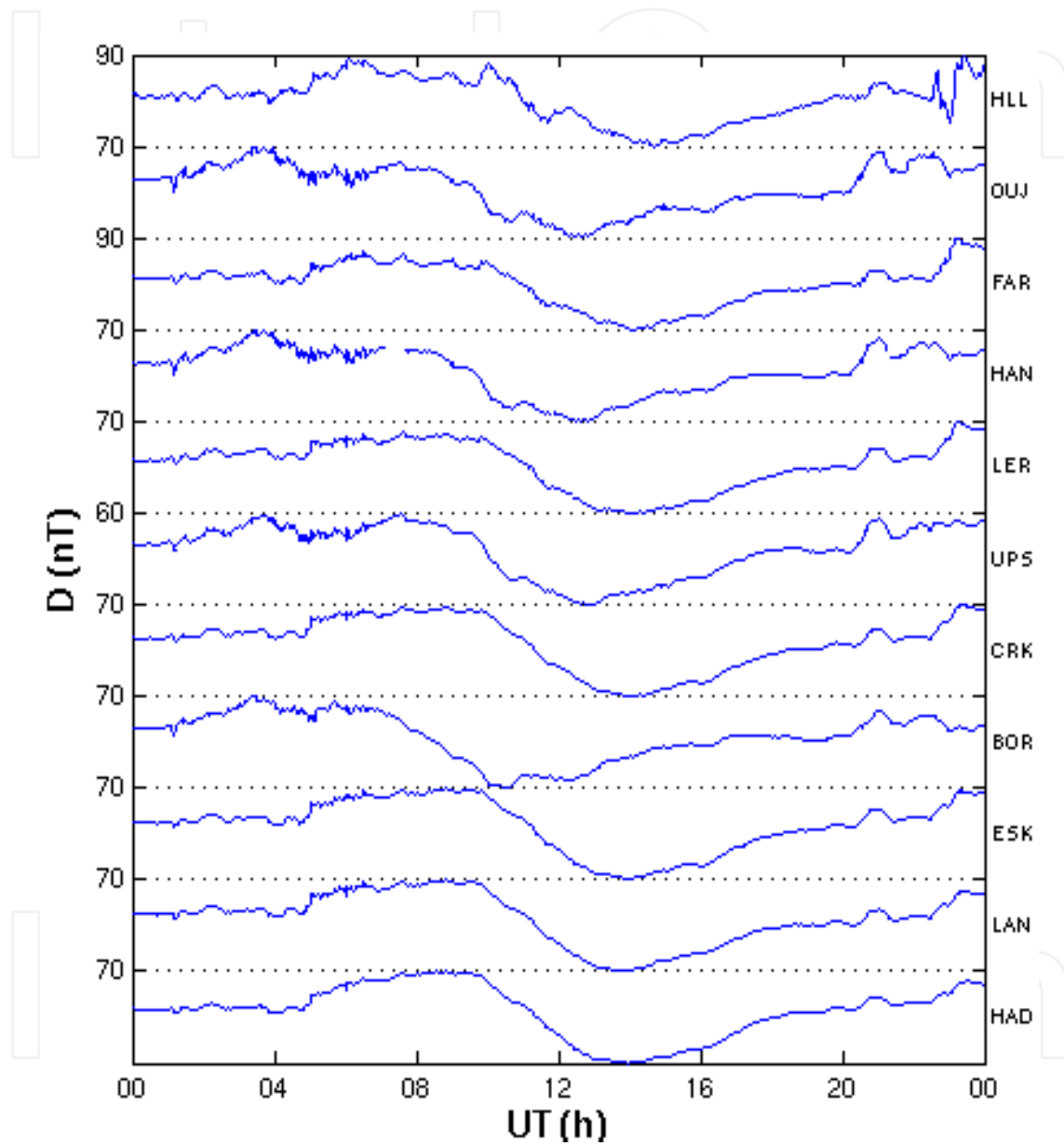


Fig. 10. D-Component SAMNET Magnetogram.

The Z component is plotted for all SAMNET stations for the particular day of measurement in Fig. 11.

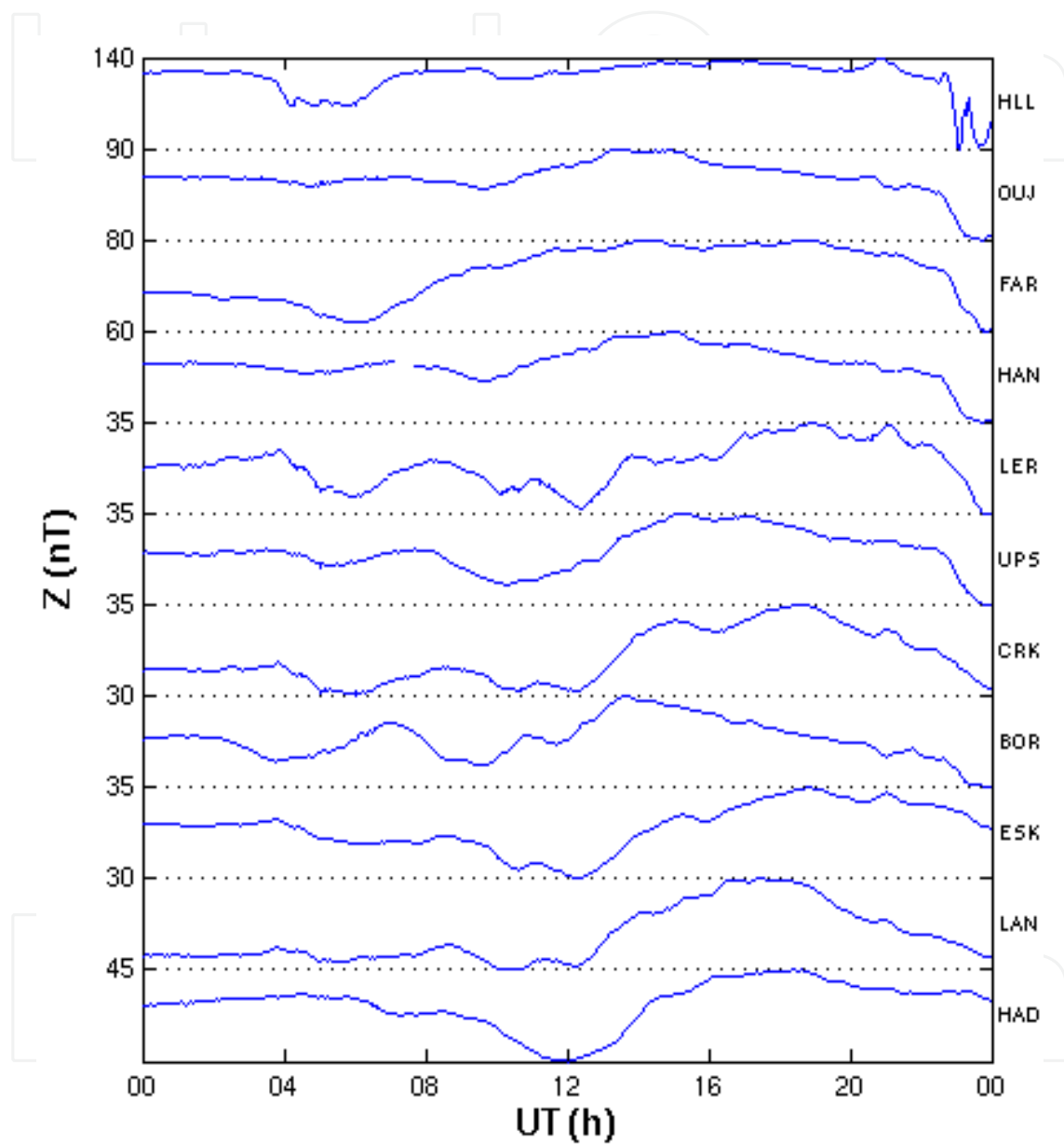


Fig. 11. Z-Component SAMNET Magnetogram.

The H, D and Z components are similarly plotted for DIMAGORAS in Fig. 12.

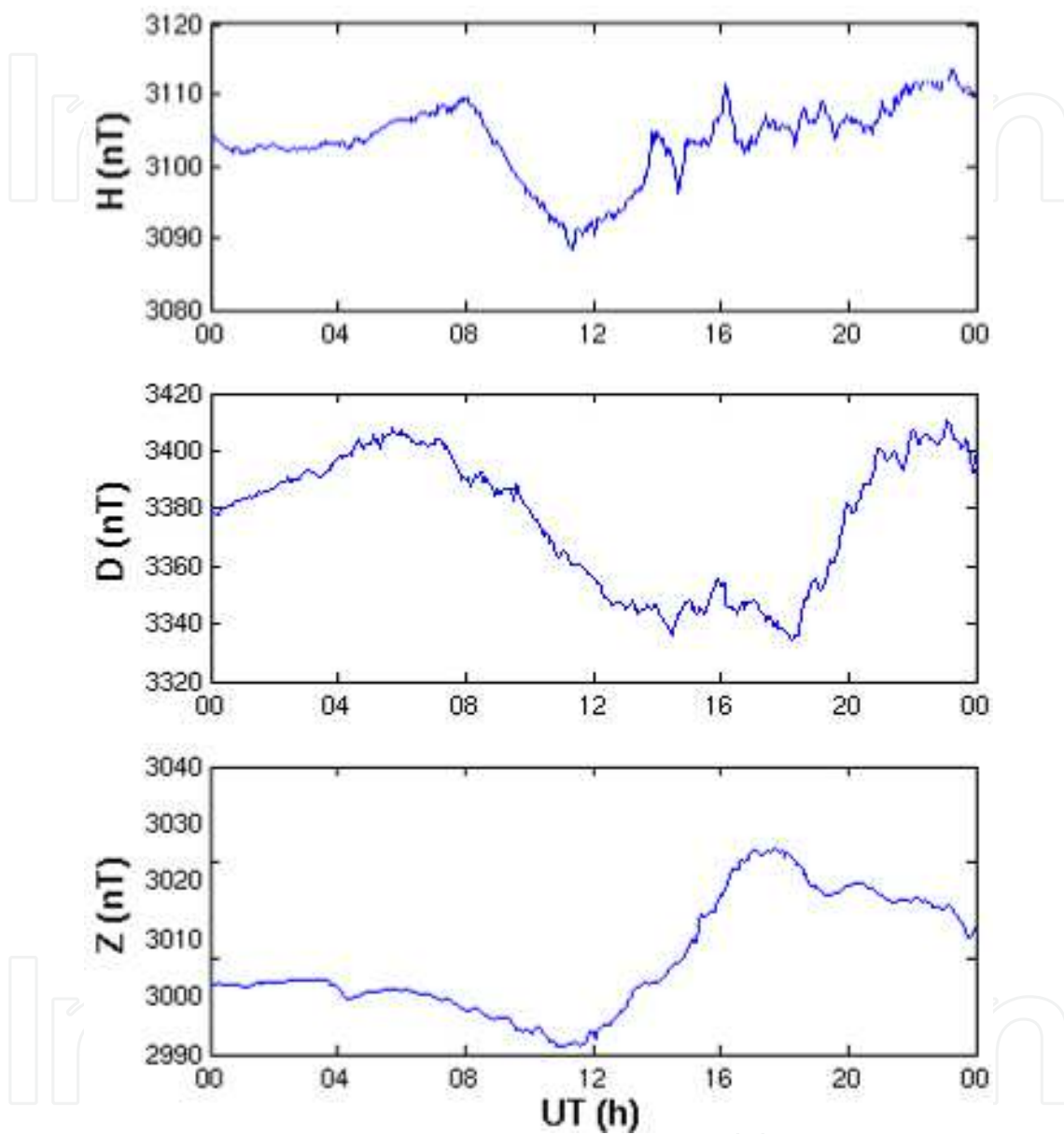


Fig. 12. H, D and Z-Components DIMAGORAS Magnetogram.

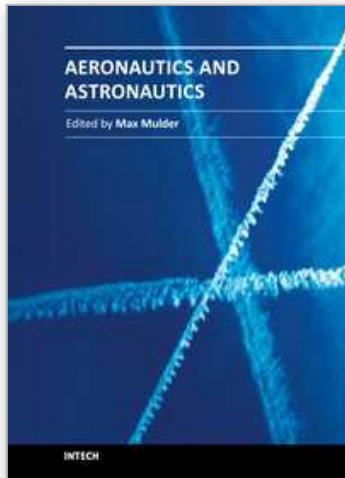
For a distant installation, the results are transferred to the central database in an automatic and unsupervised way. Automation software retrieves, at a specific time every day, the last day's data. Various methods have been tested, such as, PPP modem connection, FTP and e-mail.

## 5. Conclusion

The chapter presents a new reconfigurable magnetometer for measuring planetary fields. The scale is programmable for space field measurements. The modular design allows similar sensors' instrumentations to be quickly evaluated. The all-digital computer architecture implemented allows full control in both the analogue and digital domains. Almost all hardware functions are controlled and occasionally reprogrammed by the FPGA. The FPGA may be reconfigured approximately 20,000,000 times without any problems. 370,000 gates are required for basic operation, which is increased to 640,000 gates for optimum results. This great variation depends on the filters and DSP implementation. The minimum frequency of internal operation is 60 MHz. The system acts as a pathfinder for future space missions, since it is a replacement to existing magnetometers found in every spacecraft.

## 6. References

- Auster, H. et al. (1995). Concept and First Results of a Digital Fluxgate Magnetometer. *Measurements Science & Technology*, Vol. 7, 477-481
- Chiezi, L.; Kejik, P.; Jannosy B. & Popovic R. S. (2000). CMOS Planar 2-D Microfluxgate Sensor. *Sensors and Actuators A*, Vol. 82, 174-180
- Dekoulis, G. (2007). Novel Digital Systems Designs for Space Physics Instrumentation, *Ph.D. Thesis*, Lancaster University
- Dekoulis, G. & Honary, F. (2007). Novel Low-Power Fluxgate Sensor Using a Macroscale Optimisation Technique for Space Physics Instrumentation. *SPIE, Smart Sensors, Actuators, and MEMS III*, Vol. 6589, 65890G-1 - 65890G-8
- Dekoulis, G. & Honary, F. (2008). Novel Sensor Design Methodology for Measurements of the Complex Solar Wind - Magnetospheric - Ionospheric System. *Journal of Microsystem Technologies*, Vol. 14, No. 4-5, 475-482
- Dekoulis, G. & Murphy, N. (2008). New Digital Systems Designs for Validating the JPL Scalar Helium Magnetometer for the Juno Mission. *NASA JPL Research Report*
- Kawahito, S. et al. (1999). A Delta-Sigma Sensor Interface Technique with Third Order Noise Shaping. *Transducers Conference*, Sendai, Japan, 824-827
- Macmillan S.; Barraclough, D. R.; Quinn, J. M. & Coleman, R. J. (1997). The 1995 Revision of the Joint US/UK Geomagnetic Field Models - I. Secular Variation. *Journal of Geomagnetism & Geoelectrism*, Vol. 49, 229 - 243
- Meydan, T. (1995). Application of Amorphous Materials to Sensors. *Journal of Magnetic Materials*, Vol. 133, 525-532
- Ness, N. F. (1970). Magnetometers for Space Research. *Space Science Review*, Vol. 11, 459-554
- Pallas-Areny, R. & Webster, J. G. (1991). *Sensors and Signal Conditioning*. New York: Wiley
- Pedersen, E. B. et al. (1999). Digital Fluxgate Magnetometer for the Astrid-2 Satellite. *Measurements Science & Technology*, Vol. 10, N124-N129
- Primdahl, F. et al. (1994). Digital Detection of the Fluxgate Sensor Output Signal. *Measurements Science & Technology*, Vol. 5, 359-362
- Seidemann, V.; Ohnmacht, M.; & Buttgenback, S. (2000). Microcoils and Microrelays- An Optimised Multilayer Fabrication Process, *Sensors and Actuators A*, Vol. 83, 124-129
- (2003). SAMNET Data Collection and Processing. *Lancaster University Technical Report*



## **Aeronautics and Astronautics**

Edited by Prof. Max Mulder

ISBN 978-953-307-473-3

Hard cover, 610 pages

**Publisher** InTech

**Published online** 12, September, 2011

**Published in print edition** September, 2011

In its first centennial, aerospace has matured from a pioneering activity to an indispensable enabler of our daily life activities. In the next twenty to thirty years, aerospace will face a tremendous challenge - the development of flying objects that do not depend on fossil fuels. The twenty-three chapters in this book capture some of the new technologies and methods that are currently being developed to enable sustainable air transport and space flight. It clearly illustrates the multi-disciplinary character of aerospace engineering, and the fact that the challenges of air transportation and space missions continue to call for the most innovative solutions and daring concepts.

### **How to reference**

In order to correctly reference this scholarly work, feel free to copy and paste the following:

George Dekoulis (2011). Novel Digital Magnetometer for Atmospheric and Space Studies (DIMAGORAS), Aeronautics and Astronautics, Prof. Max Mulder (Ed.), ISBN: 978-953-307-473-3, InTech, Available from: <http://www.intechopen.com/books/aeronautics-and-astronautics/novel-digital-magnetometer-for-atmospheric-and-space-studies-dimagoras->

**INTECH**  
open science | open minds

### **InTech Europe**

University Campus STeP Ri  
Slavka Krautzeka 83/A  
51000 Rijeka, Croatia  
Phone: +385 (51) 770 447  
Fax: +385 (51) 686 166  
[www.intechopen.com](http://www.intechopen.com)

### **InTech China**

Unit 405, Office Block, Hotel Equatorial Shanghai  
No.65, Yan An Road (West), Shanghai, 200040, China  
中国上海市延安西路65号上海国际贵都大饭店办公楼405单元  
Phone: +86-21-62489820  
Fax: +86-21-62489821



© 2011 The Author(s). Licensee IntechOpen. This chapter is distributed under the terms of the [Creative Commons Attribution-NonCommercial-ShareAlike-3.0 License](#), which permits use, distribution and reproduction for non-commercial purposes, provided the original is properly cited and derivative works building on this content are distributed under the same license.

IntechOpen

IntechOpen